Climate Dynamics (2000) 16:19–34

H.-H. Syu · J. D. Neelin

ENSO in a hybrid coupled model. Part I: sensitivity to physical parametrizations

Received: 17 April 1998 / Accepted: 22 July 1999

Abstract A hybrid coupled model (HCM) for the tropical Pacific ocean-atmosphere system is used to test the effects of physical parametrizations on ENSO simulation. The HCM consists of the Geophysical Fluid Dynamics Laboratory ocean general circulation model coupled to an empirical atmospheric model based on the covariance matrix of observed SST and wind stress anomaly fields. In this two-part work, part I describes the effects of ocean vertical mixing schemes and atmospheric spin-up time on ENSO period. Part II addresses ENSO prediction using the HCM and examines the impact of initialization schemes. The standard version of the HCM exhibits spatial and temporal evolution that compare well to observations, with irregular cycles that tend to exhibit 3- and 4-year frequency-locking behavior. Effects in the vertical mixing parametrization that produce stronger mixing in the surface layer give a longer inherent ENSO period, suggesting model treatment of vertical mixing is crucial to the ENSO problem. Although the atmospheric spin-up time scale is short compared to ENSO time scales, it also has a significant effect in lengthening the ENSO period. This suggests that atmospheric time scales may not be truly negligible in quantitative ENSO theory. Overall, the form and evolution mechanism of the ENSO cycle is robust, even though the period is affected by these physical parametrizations.

1 Introduction

The El Niño/Southern Oscillation (ENSO) phenomenon, the most prominent interannual time-scale oscillation of the tropical climate system, occurs as a self-sustained cycle over the tropical Pacific Ocean due to ocean-atmosphere interaction. In this cycle, sea surface temperature (SST) anomalies cause the strengthening or weakening of the trade winds through atmospheric circulation. This phenomenon drives the ocean circulation, including currents and subsurface thermal structure, which in turn affects SST anomalies.

The observational features and evolution of ENSO events are examined in, e.g., Rasmusson and Carpenter (1982), and Deser and Wallace (1990). A "delayed oscillator" mechanism, which involves a positive feedback due to coupling and a delayed negative feedback due to ocean wave adjustment, was proposed by Schopf and Suarez (1988), Suarez and Schopf (1988), and Battisti and Hirst (1989) to explain the oscillatory nature and interannual time scale of ENSO. On the other hand, Neelin (1991), and Hao et al. (1993) showed that the time scales of ocean wave dynamics need not be essential to the interannual oscillation in some coupled regimes. Within these regimes, coupled air-sea oscillations can occur when a "fast-wave limit" is applied, in which case the delay times are eliminated from equations governing the thermocline displacement. The slow modes of the coupled system are then associated with the time derivative of the SST equation and are therefore referred to as SST modes. Schopf and Suarez (1990) and Cane et al. (1990) formulated the "fast-SST limit" to further address the ocean wave dynamics in the coupled problem. Jin and Neelin (1993a, b) and Neelin and Jin (1993) provided a unified view by showing that "fast-wave limit" and "fast-SST limit" are the two extremes in the coupled flow regime. Elsewhere in the parameter space, the leading modes are best characterized as mixed SST/ocean-dynamic modes.

One of the well-known features of the ENSO phenomenon is its irregular period of 2–7 years. Two major sources of ENSO irregularity are the deterministic chaos within the nonlinear dynamics in the coupled system and the uncoupled atmospheric weather noise. In this work, we address only ENSO behavior when no atmospheric

H.-H. Syu
Jet Propulsion Laboratory,
California Institute of Technology, Pasadena, CA 91109, USA

J. D. Neelin (✉)
Department of Atmospheric Sciences, University of California, Los Angeles, Los Angeles, CA 90095, USA
E-mail: neelin@atmos.ucla.edu

weather noise is included. Without the weather noise, the ENSO periods simulated in some ENSO models (e.g., Anderson and McCreary 1985; Battisti 1988; Barnett et al. 1993; Syu et al. 1995) are found to be regularly locked into certain interannual intervals. Frequency locking is known as a resonant response occurring in nonlinear systems of coupled oscillators between modes or oscillators coupled to periodic external forces when the interaction between them is strong enough (Iooss and Joseph 1990). In the quasi-periodic route, it is organized as a "devil's staircase" structure, in which the inherent frequency of the system locks onto a sequence of steps of rational fractions of the external frequency (Bak 1986; Jensen et al. 1984). Overlapping of these frequency locked steps, caused by increased nonlinearity, leads to chaos due to the erratic jumps between the various overlapping resonances. The mechanism of frequency locking and the transition to chaos in ENSO (Jin et al. 1994, 1996; Tziperman et al. 1994, 1995; Chang et al. 1994, 1995) also provides an explanation for the phase-locking of ENSO events to the seasonal cycle, as observed by Rasmusson and Carpenter (1982) and found in many ENSO simulations.

Jin et al. (1994) used the surface-feedback parameter, which affects ENSO period, to construct a "devil's staircase" of frequency locked steps. By systematically changing both the surface-feedback parameter and the coupling parameter, Jin et al. (1996) mapped out a "devil's terrace" structure of frequency locked steps and chaotic regimes as a function of both parameters, in a stripped-down version of the Cane and Zebiak (CZ hereafter) model (Cane and Zebiak 1985, Zebiak and Cane 1987). They found that the locking tends to occur in frequencies close to the inherent ones but occurs over broader areas for the integer periods. Chaos can occur by overlapping of the frequency locked regimes. At realistic coupling, paths from strongly locked solutions to chaotic solutions are more easily obtained by changing the inherent ENSO frequency rather than by varying the coupling strength. In the Jin et al. (1994, 1996) model, the surface-feedback parameter governs the inherent periods in an inverse relationship. This relationship is also indicated by the previous version of the hybrid coupled model (HCM) results (Syu et al. 1995), with the parameter of surface-layer feedback replaced by the mixing coefficient in the ocean mixed layer. Two vertical mixing schemes were compared in Syu et al. (1995), the Pacanowski and Philander (1981) vertical mixing scheme (PP scheme hereafter) and a modified version of the Richardson-number-dependent PP scheme (B. Blanke 1993, personal communication; Mod-Ri scheme hereafter, referred to as the MVM scheme in Syu et al. 1995). The modified scheme allows stronger vertical mixing in the ocean surface layer than the PP scheme, thus reducing the surface-layer feedbacks and increasing the inherent coupled period from 21 months to 27.6 months. However, when the seasonal cycle is present, both schemes still fall into the nearest integer frequency regime: the quasi-biennial regime. This is the strongest frequency locking regime, since both nonlinear and linear interactions can lead to that regime.

In Syu et al. (1995), a steady-state atmosphere was assumed. The atmospheric adjustment time was completely neglected due to its small time scale compared to the oceanic adjustment time scale. Although this is a reasonable assumption from the point of view of scaling analysis and many simple atmospheric models adopt this approximation, the treatment is over-simplified because it excludes any spin-up time for real atmospheric processes, e.g., large-scale circulation, evaporation and cumulus convection processes. Here a modification to include a representation of the atmospheric spin-up time scale in the HCM is presented to examine the impacts to the coupled behavior.

Phase-locking behavior is addressed in Neelin et al. (1999). This study focuses on ENSO simulation and the effects of physical parametrizations on ENSO period (part I), and ENSO prediction (part II). Part I is organized as follows. In Sect. 2, we briefly describe the hybrid coupled model used in this work. Section 3 discusses the effect on ENSO periods given by two factors, the ocean vertical mixing scheme and atmospheric time scale. Section 4 presents the model performance of the standard version of the hybrid coupled model. Conclusions are given in Sect. 5.

2 Hybrid coupled model

The class of "hybrid coupled models" consists of an ocean general circulation model (OGCM) coupled to a simplified atmospheric model, representing the steady-state atmospheric response to oceanic boundary conditions. In the coupled system, due to the different time scales of ocean and atmosphere, the atmosphere can be effectively treated as a rapidly adjusting component, while the ocean has the memory of the system. For the tropical domain, temporal variability in the system is attributed primarily to coupling. The HCM is thus able to describe the coupled system in the tropical domain and yields an understanding of the inherent properties of the coupled system. Among coupled models with several complexity, the HCM can describe the nonlinearity of the coupled system better than intermediate and simple models, while it is more economical to use. In addition, it is easier to distinguish the effects due to the oceanic and atmospheric components in an HCM compared to a coupled GCM.

The type of HCM presented here uses an empirical atmospheric component, based on the assumption that for monthly or longer time scales, contemporaneous correlation between wind stress and sea surface temperature (SST) is associated with the atmosphere's rapidly adjusted nonlocal response to the SST pattern throughout the basin. As first introduced by Latif and Villwock (1990), this empirical atmosphere approach is also used by several studies, e.g., Latif and Flügel (1991), Barnett et al. (1993) and Balmaseda et al. (1994).

The HCM used here is similar to the standard version in Syu et al. (1995), which has applications also in Waliser et al. (1994) and Blanke et al. (1997). The empirical atmospheric model is estimated from observations using a singular value decomposition (SVD) technique. The model contains the first seven SVD modes of the SST-pseudo-stress covariance matrix calculated from the time series of observed monthly mean Reynolds' SST (Reynolds 1988) and Florida State University (FSU) pseudo-stress fields (Legler and O'Brien 1984) over a 19-year period from January, 1970 through December, 1988. The mean seasonal cycle is removed from the data set before calculating the SVD modes (as the SVDI model described in Syu et al. 1995). A set of re-estimated SVD modes is used in the current version, which is slightly different from the previous version quantitatively, but most qualitative features are maintained. In addition to the re-estimated SVD modes, the atmospheric time scale (atmospheric spin-up time), which was neglected in the previous version, is parametrized in the current version, albeit crudely, within coupling procedures. The inclusion of the atmospheric spin-up time turns out to influence the period of the ENSO cycle. Details of this modification and its effects are addressed in Sect. 3.2.

The surface heat flux parametrization as formulated by Oberhuber (1988) includes observed heat flux (as estimated from COADS data) and a linearized negative feedback term, resulting from the tendency of fluxes out of the ocean surface to increase with increasing SST. The negative feedback term is calculated according to Seager et al. (1988) to include the change of atmospheric boundary layer moisture associated with SST.

The OGCM is a version of the GFDL modular ocean model (Pacanowski, Dixon and Rosati 1991, personal communication) based on Cox (1984). The ocean domain covers the Pacific basin from 30°S to 50°N, 130°E to 80°W, with continents. A vertical resolution of 27 levels is used, with 10 levels in the upper 100 m. A solar-penetration algorithm (Paulson and Simpson 1977) is adopted in the model. The vertical mixing scheme applied is the Mod-Ri scheme. The Mod-Ri scheme uses a similar Richardson-number-dependent algorithm as in the Pacanowski and Philander (1981, PP hereafter) PP scheme, but re-estimates the profile of vertical mixing coefficients according to observations (Peters et al. 1988). The new relationship brings in more mixing in high turbulence regions and less mixing in low turbulence regions than does the PP scheme. A more detailed description of the Mod-Ri vertical mixing scheme used in the model, is documented in Appendix A. It is well known that the PP scheme only parametrizes the ocean interior mixing associated with shear instability. The Mod-Ri mixing scheme likewise also parametrizes only the ocean interior mixing. A simple ocean boundary layer (surface mixed layer) parametrization, as employed in Latif et al. (1994), is thus also included in the current version. The formulation and effects of the surface-layer mixing are discussed in Sect. 3.1.

3 Effects on ENSO period

As mentioned in Introduction and Sect. 2, two effects previously omitted in the HCM, surface wind mixing and atmospheric time scale, are included in the current model. They are found to have effects on the coupled periods. These two parametrizations and the coupled results are described.

3.1 Surface-layer mixing scheme

Both the PP scheme and the Mod-Ri scheme, and indeed most ocean vertical mixing schemes, parametrize only the ocean interior mixing processes and not the boundary-layer mixing. The atmosphere and ocean communicate with each other via their respective planetary boundary layers. The importance of including an ocean boundary-layer, which has properties distinct from the ocean interior, has been demonstrated in Large et al. (1994). Here we follow Latif et al. (1994) to include a simple surface mixed-layer parametrization, in which a constant mixing coefficient is added in the surface mixed layer in addition to the vertical mixing given by the Mod-Ri scheme, in order to parametrize surface wind mixing due to the increased turbulent kinetic energy.

A key factor that needs to be determined in the surface mixed-layer parametrization is the depth of the surface mixed layer. We adopt a commonly used definition to determine the depth of the surface mixed layer, for any given layer, if the temperature difference between the layer and the surface is less than 0.5 °C, the layer is considered to be part of the surface mixed layer. The turbulent mixing within the surface mixed layer is given by adding an additional vertical diffusivity/viscosity coefficient to the value calculated by the vertical mixing scheme, PP in Latif et al. (1994) and Mod-Ri in the HCM. Levels beneath the determined surface mixed layer have no such additional vertical mixing added. Specifically,

$$\nu = \begin{cases} \nu_b + \nu_{sml}, & \text{if } |(\mathrm{T} - \mathrm{T}_0)| \le 0.5 \\ \nu_b, & \text{if } |(\mathrm{T} - \mathrm{T}_0)| > 0.5 \end{cases}$$

where ν is the total mixing coefficient, ν_b is the mixing coefficient given by the chosen vertical mixing scheme and ν_{sml} is the additional mixing coefficient for the surface-layer parametrization, which is constant throughout the surface layer. The ν_{sml} chosen in Latif et al. (1994) is 20 cm^2/s. Since the Mod-Ri scheme gives stronger vertical mixing than the PP scheme in the mixed layer, we reduce the constant surface mixing to 10 cm^2/s in the HCM.

An uncoupled OGCM integration is first carried out to evaluate the performance of the surface-layer parametrization. The OGCM is spun up from rest and forced by observed seasonal-varying climatological wind stress and heat flux, with initial temperature and salinity profiles from the Levitus (1982) climatology from January.

The overall spatial and temporal features of the simulated seasonal cycle are quite realistic using the surface-layer mixing parametrization. The impacts of the surface-layer mixing are: the strength of zonal current seasonal variation (figure not shown) is slightly reduced, as a result of the inverse relationship with vertical mixing strength. The seasonal variation of vertical currents (figure not shown) in the western Pacific is increased, probably due to reduction of stratification by stronger mixing. The increased effects of mixing in the western Pacific are also reflected in the zonal-vertical temperature field. Figure 1 illustrates the longitude-depth section along the equator of annual averaged total temperature fields of the MSC with the surface-layer parametrization. The bottom of the homogeneous temperature layer is around 100-m in depth and the horizontal temperature gradient in upper ocean is comparable with observations. Figure 2a–d displays the difference between the longitude-depth temperature fields of both vertical mixing schemes for four seasons. The thermocline is deepened both east and west of the basin with the surface-layer parametrization in all seasons, especially in the western Pacific, as is consistent with the enhanced vertical velocity field. The seasonal variation is more clearly seen in the eastern Pacific. Immediately below the positive impact region around 60–100 m, a band with negative impact is shown across the basin, also in all seasons. A stronger vertical temperature gradient within the thermocline is thus implied.

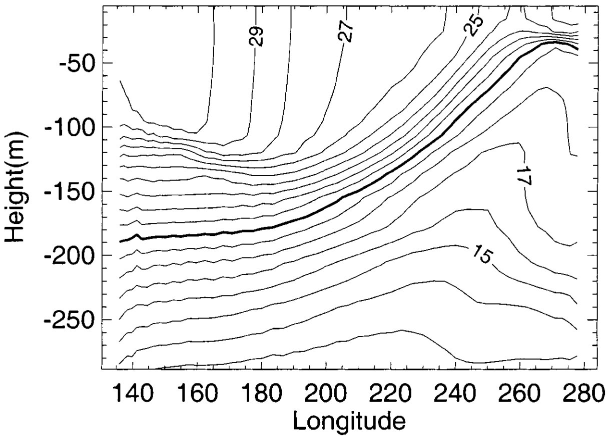

Fig. 1 Longitude-depth annual-mean temperature field (along the equator) of an uncoupled OGCM simulation with the surface mixed-layer parametrization and seasonal varying boundary conditions. Contour interval is 1 °C; the *thick solid line* represents 20 °C isotherm

With stronger surface mixing, SST is slightly lower in the western Pacific.

3.1.1 Coupled inherent variability and seasonal cycle effects on ENSO

We first examine inherent ENSO variability in absence of the seasonal cycle. The SST and zonal wind stress anomaly fields along the equator for the last 21 years of a 30-year coupled simulation are displayed in Fig. 3a, b, with the surface-layer parametrization and annual-averaged boundary conditions. Anomalies are with respect to the time average of the run. The coupled inherent period is approximately 3 years. The same simulation for the Mod-Ri scheme without the surface-layer parametrization results in a 2.5-year inherent period (Fig. 4a). The longer period with the surface-layer parametrization is consistent with that indicated in Jin and Neelin (1993a, b) and Neelin and Jin (1993), in which weaker

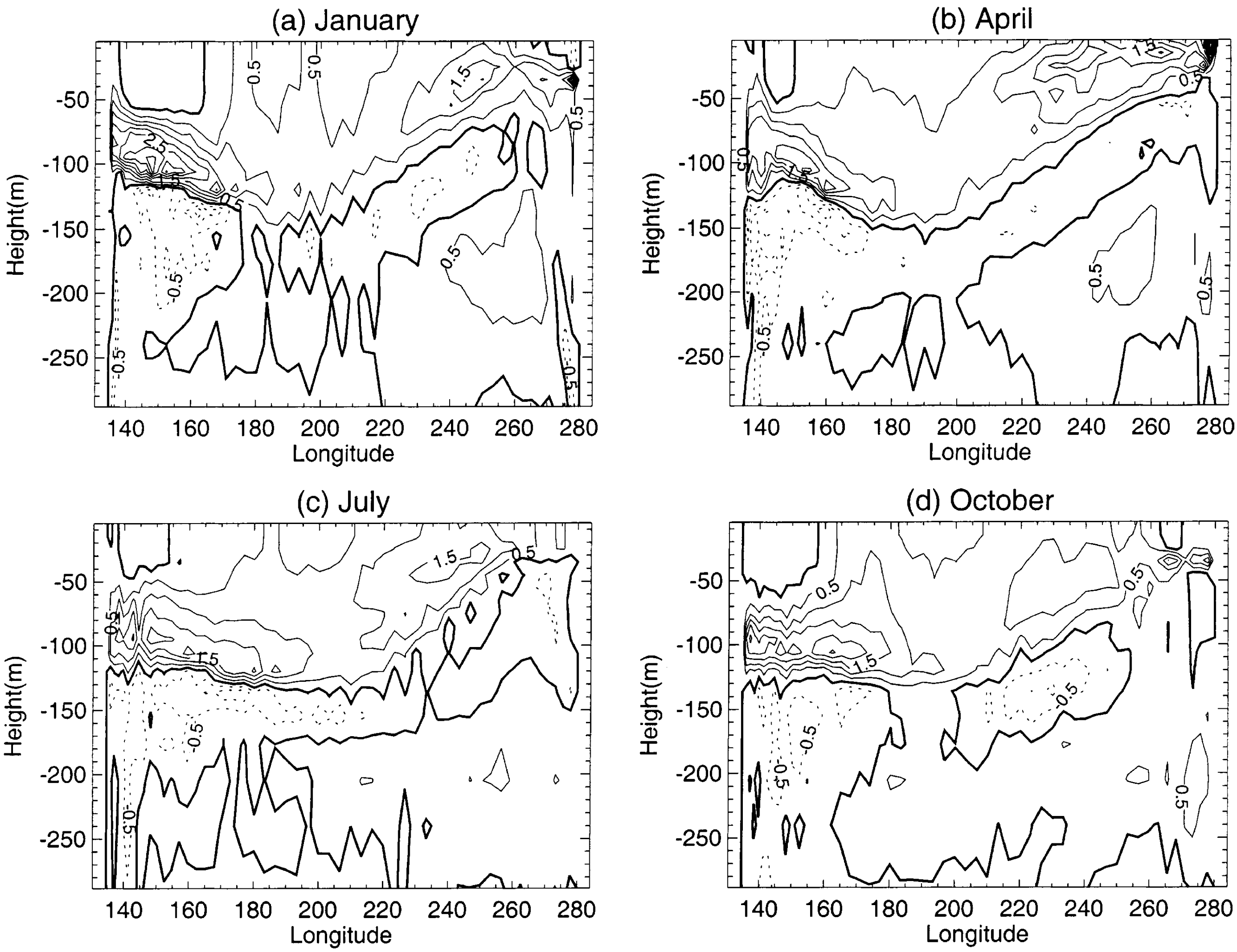

Fig. 2a–d Temperature difference (longitude-depth section along the equator) between the mean seasonal cycles (MSC) of uncoupled OGCM simulations with and without the surface-layer parametrization while seasonal varying boundary conditions are prescribed. Difference of four monthly means of **a** January, **b** April, **c** July and **d** October, representing the four seasons, are shown. Contour interval is 0.5 °C and *dashed* (*solid*) *lines* represent negative (positive) difference from the case without the surface-layer parametrization

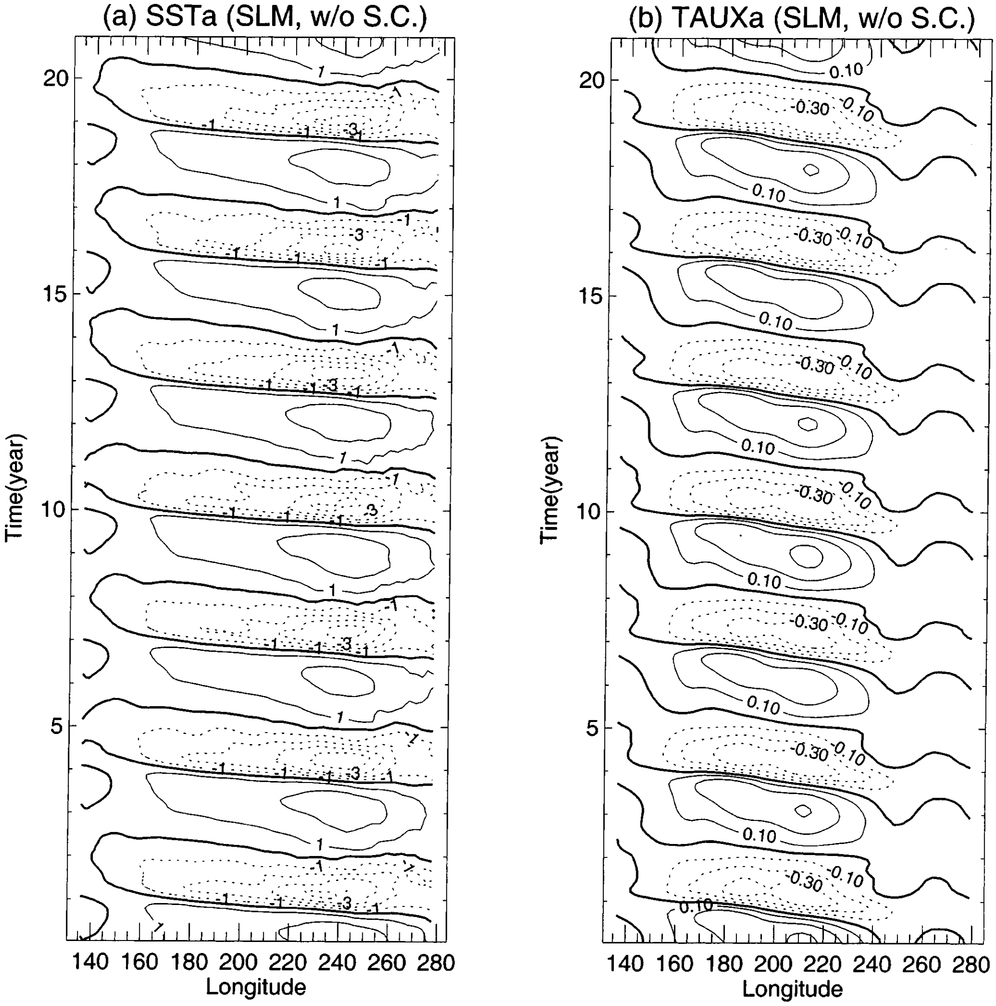

Fig. 3a, b Time-longitude anomaly fields (with the annual mean removed) of **a** SST and **b** zonal wind stress along the equator for the last 21 years of a 30-year coupled simulation with the surface-layer parametrization in the absence of the seasonal cycle. Contour interval is 1 °C for SST field and 0.1 dyne/cm^2 for wind stress field. *Dashed lines* represent negative anomalies and *solid lines* represent positive anomalies. A three-point smoothing is applied to all time-longitude diagrams in this work

surface-layer feedbacks, corresponding to stronger vertical mixing in the HCM, result in longer coupled periods. The deeper mixed layer, caused by stronger mixing (Figs. 1 and 2), may also increase the coupled time scale. Spatial distribution and temporal relationship between SST and zonal wind stress anomaly fields are similar in both cases. The amplitude of inherent ENSO variability for the case with the surface-layer mixing are larger than for the case without especially for cold phases. Also, with the simple surface-layer parametrization, the ocean seems to be more sensitive to local wind forcing over the central and western Pacific.

In presence of the seasonal cycle, the ENSO time evolution is slightly modified. Figure 5a and b presents the SST and zonal wind stress anomalies, with respect to the mean seasonal cycle (MSC) for the last 21 years of a 30-year coupled simulation with the surface-layer parametrization, while the seasonal cycle is prescribed through climatological wind stress and heat flux fields and ocean climatology. Figure 4b shows the same case as in Fig. 5a, but without the surface-layer parametrization. The average interannual variability is 3 years for the case with the surface-layer parametrization and 2.5 years (2 ENSO events in 5 years) for the case without; both are close to their respective inherent periods. The inclusion of surface mixing not only gives longer inherent coupled periods, but also moves the coupled system to a lower frequency regime when the seasonal cycle is involved, consistent with the intermediate model results of Jin and Neelin (1993a, b), Neelin and Jin (1993) and Jin et al. (1994). In addition to the longer period, the case with the surface-layer parametrization (Fig. 5a) has slightly stronger amplitudes in warm phases, much stronger amplitudes in cold phases, and broader warm periods compared to the case without (Fig. 4b). The spatial distribution and temporal relationship among fields with the seasonal cycle are reasonably similar to the cases without the seasonal cycle and thus are not described in detail here.

Note that the results obtained with the Mod-Ri scheme without the surface-layer parametrization are locked to a sequence of 2-year and 3-year cycles, as opposed to the quasi-biennial frequency locking obtained in Blanke et al. (1997) and Syu et al. (1995), using a version very similar to our current model, when the seasonal cycle is involved. The sensitivity can be partly attributed to the re-estimated atmospheric SVD model which is slightly different from that used in Blanke et al.

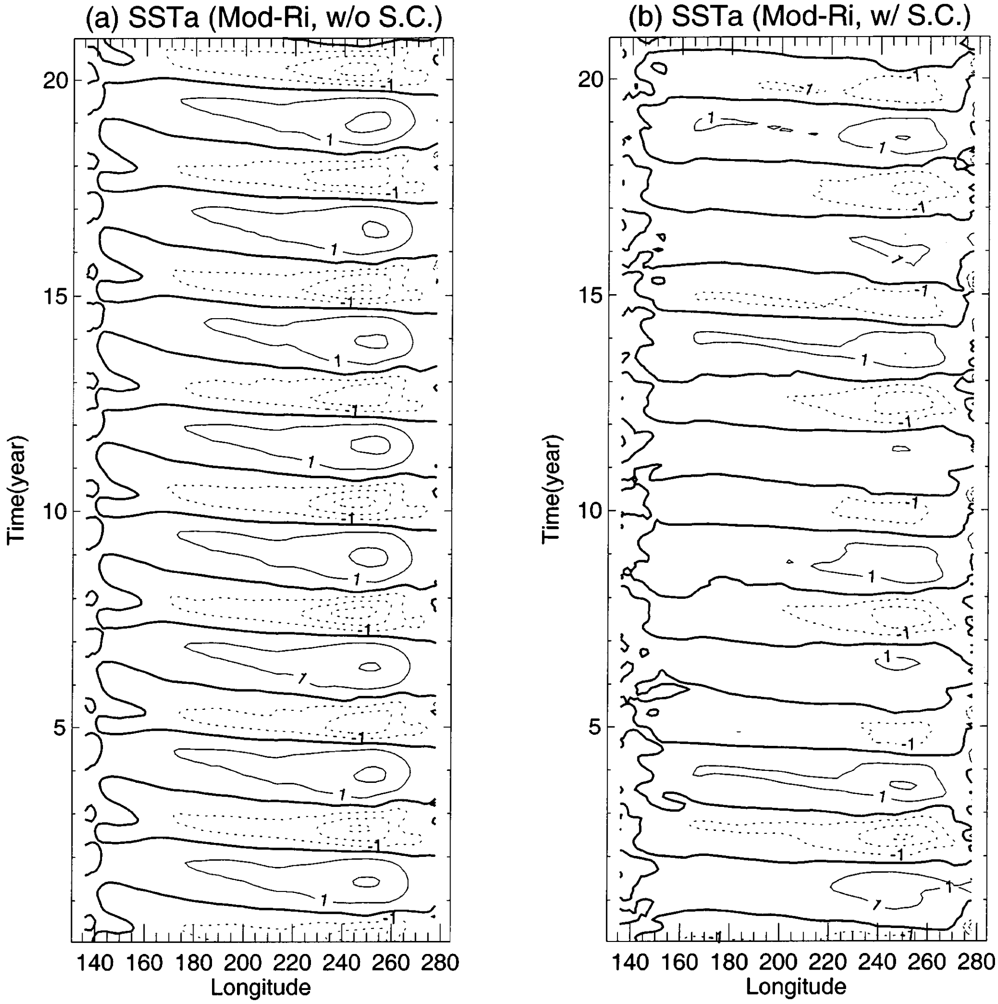

Fig. 4a, b Time-longitude SST anomaly fields of the last 21 years of 30-year coupled simulations **a** without the seasonal cycle (with time-mean removed) and **b** with prescribed seasonal-varying boundary conditions (with the MSC removed) along the equator for the case with the Mod-Ri vertical mixing scheme (without the surface-layer parametrization). Contour interval is 1 °C. *Dashed lines* represent negative anomalies and *solid lines* represent positive anomalies

(1997) and Syu et al. (1995), although the difference is so small that we did not expect to see any impact on the ENSO simulations. The sensitivity is also ascribed to the strength of the coupling coefficient and the coupling approach we chose. In Blanke et al. (1997), for example, a stronger coupling coefficient is used (1.2 versus 1.0). When we increase the coupling coefficient to 1.2 with the current SVD model, the simulated ENSO cycles also fall into QB frequency regime more easily.

3.2 Role of atmospheric time scale

The atmospheric spin-up time is crudely represented by coupling the atmosphere to the weighted averages of SST anomalies, exponentially decaying with lag time from present, instead of parametrizing the atmospheric model as responding to the current SST anomalies at each coupling time step.

3.2.1 Formulation

The wind stress anomaly is calculated as the following:

$$\tau_{x,y} = A(T_{avg}) \tag{1}$$

where $\tau_{x,y}$ represents zonal and meridional wind stress anomalies, A represents the atmospheric model and T_{avg} is the weighted SST average,

$$T_{avg} = \sum_{j=0}^{\infty} W_j \cdot T^{n-j} \ , \tag{2}$$

where W_j is the weighting function,

$$W_j = (1 - e^{-\Delta t/\tau}) \cdot e^{-j\Delta t/\tau}$$

T^{n-j} is anomaly at coupling time step n–j, representing the backward time integral, Δt is the coupling interval, one day in our case, and τ is the chosen atmospheric spin-up time scale. Equation (2) can also be written as

$$T^n_{avg} = aT^n + bT^{n-1}_{avg} \ ,$$

$$a = 1 - e^{-\Delta t/\tau} \ ,$$

$$b = e^{-\Delta t/\tau} \ . \tag{3}$$

This formulation greatly simplifies the coding process, because Eq. (3) requires only two variables to be stored, SST anomaly at the current coupling time step, T^n, and the weighted SST anomaly from the previous coupling time step, T^{n-1}_{avg}.

Fig. 5a, b Same as in Fig. 3, but with prescribed seasonal-varying boundary conditions and the MSC removed

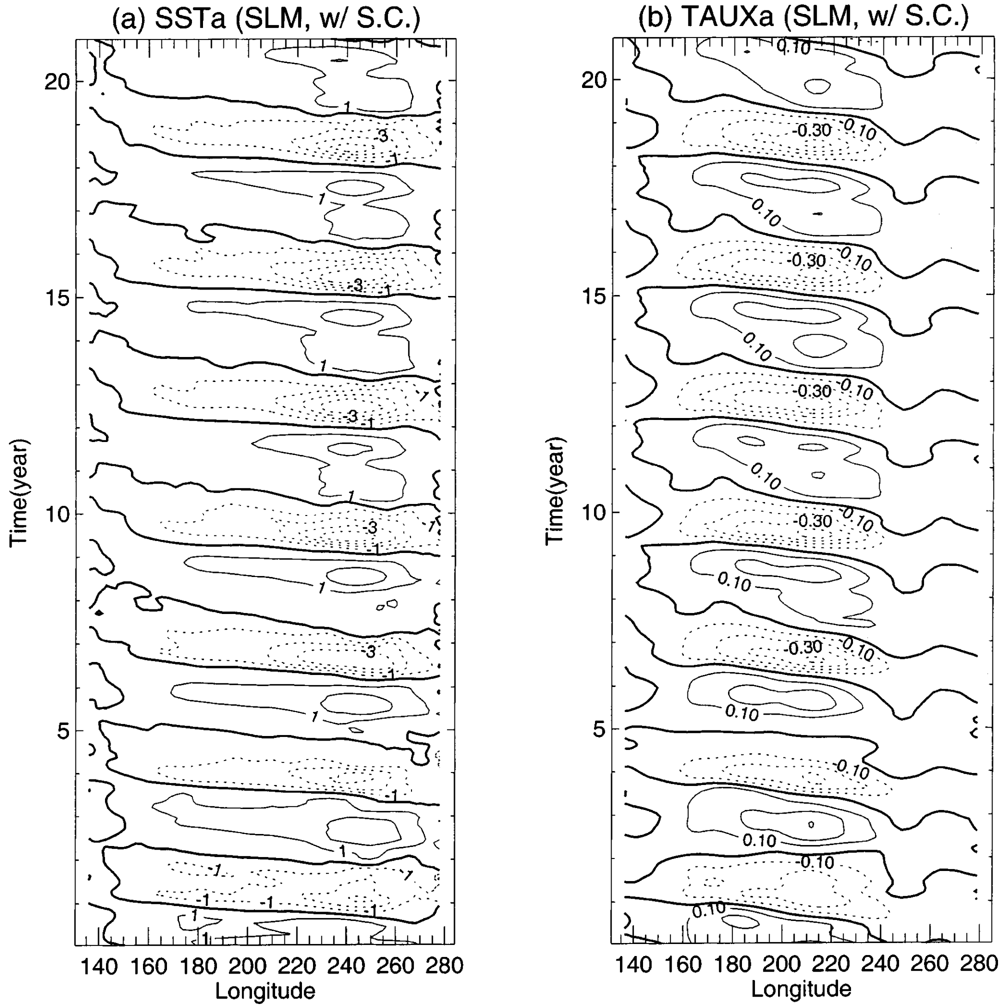

A simple diagram to illustrate the weighting function for a case with one-day coupling interval and 60-day atmospheric spin-up time is shown in Fig. 6. This exponential weighting function basically gives a smoother curve to the discrete coupling information exchange between the atmosphere and the ocean.

3.2.2 Wind field analysis

Figure 7a–d shows reconstructed zonal anomalous wind fields from the 1978-1993 observed Reynolds' SST anomaly (with respect to its MSC) and the re-estimated SVD atmospheric model, for the case without the atmospheric spin-up time parametrization and the cases including the spin-up time scale of 30, 60 and 90 days, respectively. The inclusion of the atmospheric spin-up time mainly smooths the zonal wind anomaly fields. Although slight changes of temporal and spatial distribution and amplitudes are obtained, no noticeable lag is found and major features in all aspects are retained as compared with the observations (FSU pseudo-stress). As the atmospheric spin-up time is increased, a stronger smoothing effect is obtained. The meridional wind field

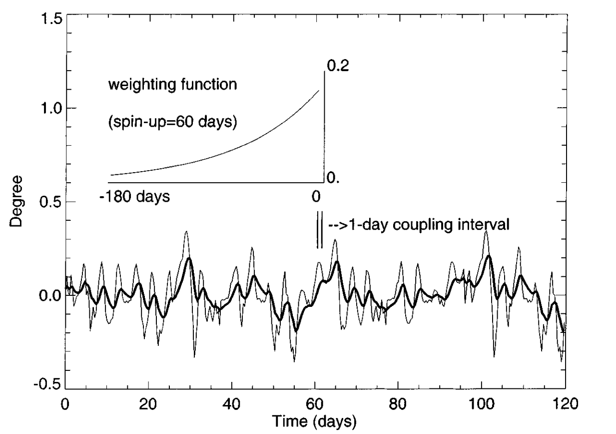

Fig. 6 Schematic diagram for the inclusion of the atmospheric spin-up time effect (*thick curve*) applied to SST output from a case with one-day coupling interval (*thin curve*). The weighting function applied for the case with a 60-day spin-up time scale is illustrated in the *left upper part* of the figure

(figures not shown) shows similar effects when the atmospheric spin-up time is included.

This is a very crude parametrization compared to the complicated atmosphere parametrizations used in GCMs

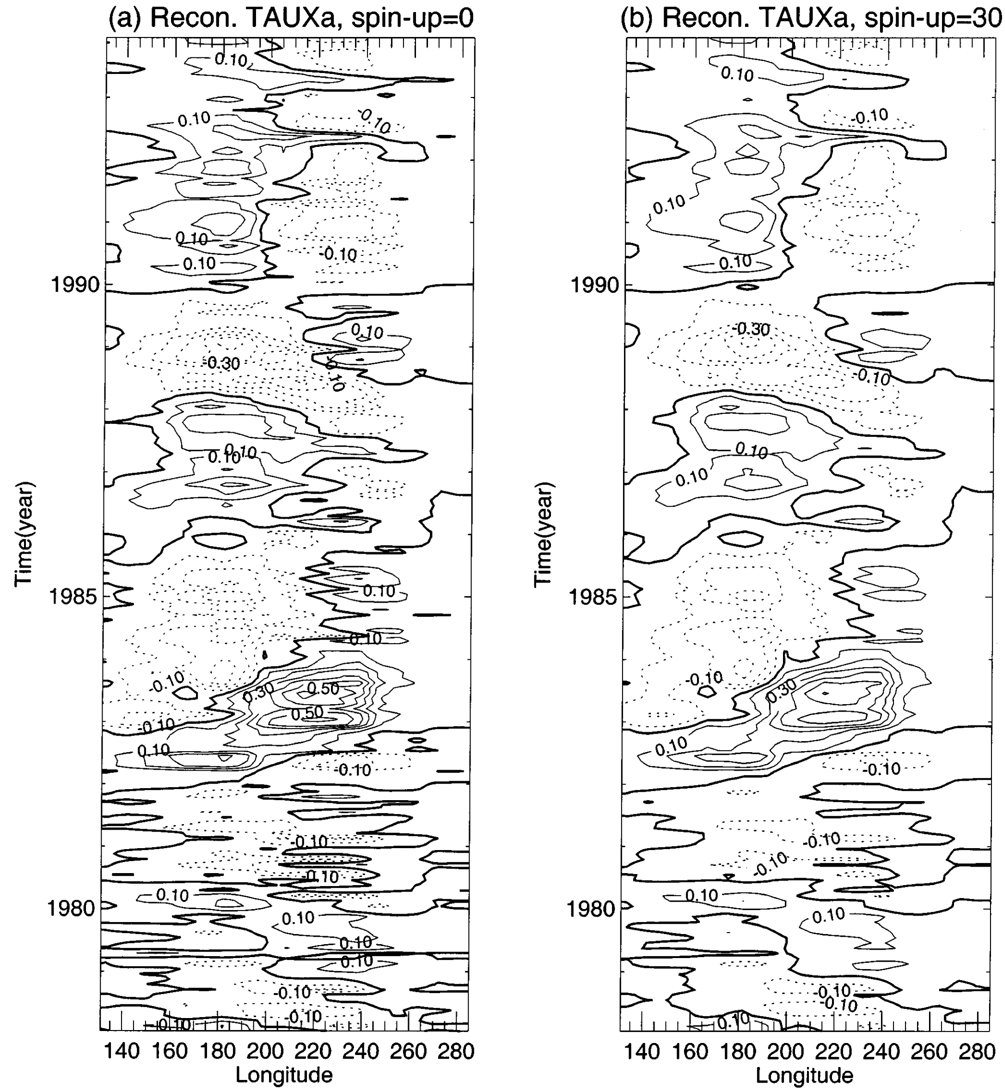

Fig. 7a–d Time-longitude reconstructed zonal stress anomaly fields with **a** no atmospheric spin-up time parametrization, **b** atmospheric spin-up time of 30 days, **c** atmospheric spin-up time of 60 days and **d** atmospheric spin-up time of 90 days from the Reynolds SST data set from 1978–1993 and the re-estimated SVD models. Contour interval is 0.1 dyne/cm^2 for all cases. *Dashed lines* represent negative values and *solid lines* represent positive values

or the real atmospheric circulation process, including for example, cumulus convection processes, with a short time scale in the deep convection area and longer time scales elsewhere, boundary-layer convergence forced by horizontal SST gradient, horizontal adjustment by wave processes either dry or interacted with convection. In this simple formulation to recover the atmospheric time scale, spatial effects are neglected and the exponential expression is assumed only because it simplifies the coding process. However, it gives significant effects on the ENSO period.

3.2.3 Inherent variability and sensitivity

To understand the effect of the atmospheric spin-up time on the coupled inherent variability with both vertical mixing schemes (with and without the surface-layer mixing scheme in addition to the Mod-Ri scheme), experiments with various atmospheric spin-up times for each mixing scheme are carried out as sensitivity studies. Figure 8 shows NINO3 indices (averaged SST anomaly over the eastern equatorial Pacific box from 150°E to 90°W, 5°S to 5°N) of 30-year coupled runs with no atmospheric spin-up effect (dashed curve) and atmospheric spin-up times of 30 (dotted curve), 60 (gray solid curve) and 90 (black solid curve) days, for the case with the surface-layer parametrization in absence of the seasonal cycle. Figure 9 shows the same analysis but for the case without the surface-layer parametrization. The coupled inherent periods are 3.0, 3.35, 3.71 and 4.05 years (with zero, 30-, 60- and 90-day atmospheric spin-up times, respectively) for runs with the surface-layer parametrization, and correspondingly, 2.5, 2.8, 3.1 and 3.3 years for the case without the surface-layer parametrization. The tendency to obtain a longer coupled inherent period with longer atmospheric spin-up time is suggested with both mixing schemes. Also, the cases with the surface-layer parametrization obtain longer coupled inherent periods than those without. Combin-

Fig. 7a–d (cont)

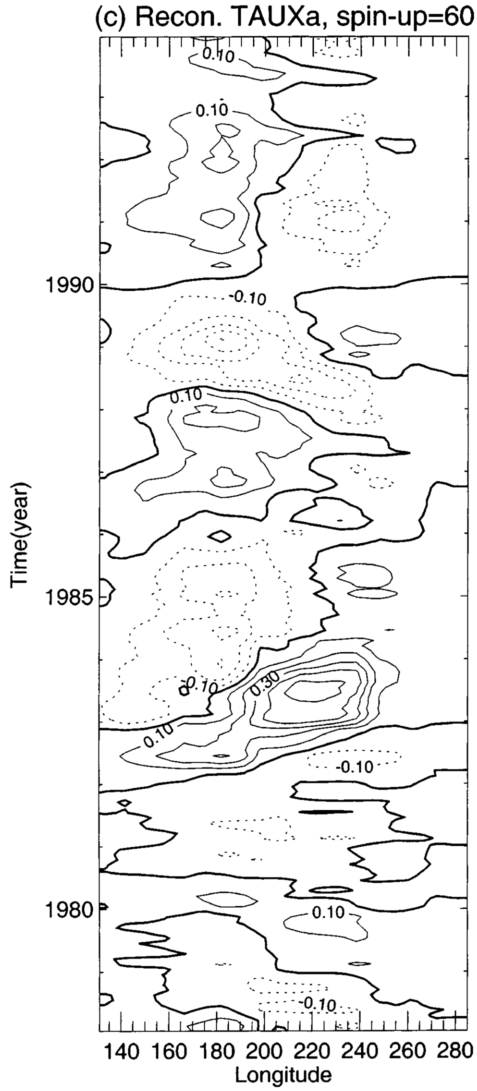

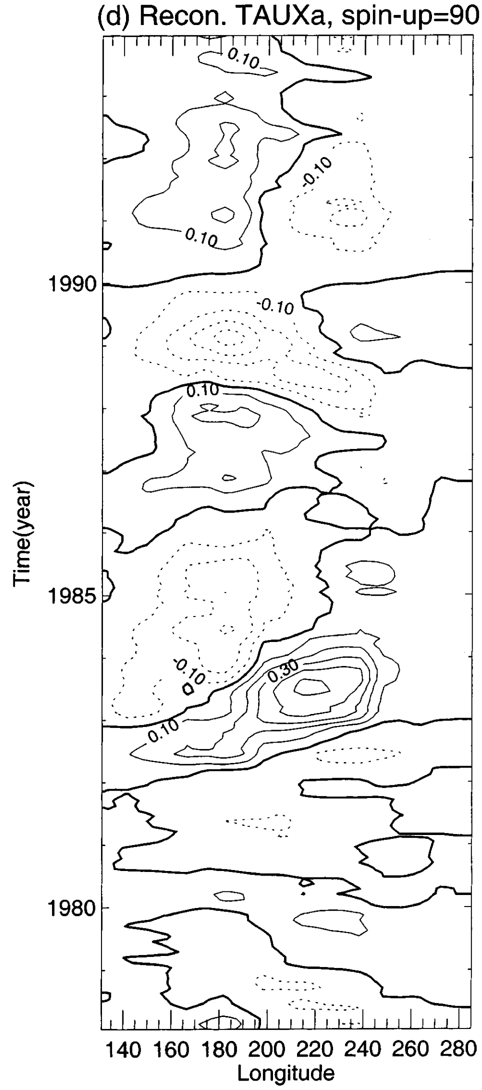

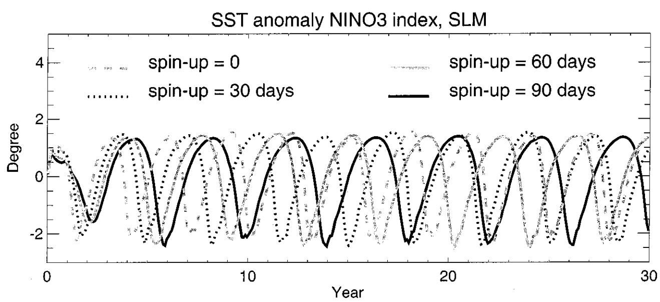

Fig. 8 Anomalies of the NINO3 SST index (SST averaged over the equatorial eastern Pacific area from 5°S to 5°N and 90°W to 150°W) for coupled simulations with the surface-layer parametrization and without the atmospheric spin-up time parametrization (*dashed curve*), with the atmospheric spin-up time scale of 30 days (*dotted curve*), with the atmospheric spin-up time of 60 days (*gray solid curve*), and with the atmospheric spin-up time of 90 days (*black solid curve*). No seasonal cycle is included in these cases

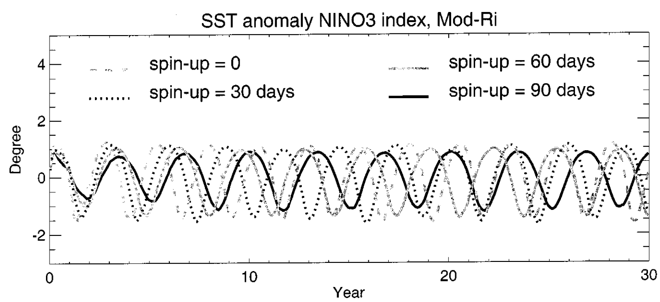

Fig. 9 Same as in Fig. 8, except for the case without the surface-layer parametrization

ing both mixing and atmospheric spin-up time effects, the longest inherent period among all cases is 4.05 years at the atmospheric spin-up time of 90 days.

Amplitudes for the case with the surface-layer mixing scheme are overall larger than those for the case without. The time scale of coupled oscillations is dominated mainly by the ocean, e.g., through ocean dynamics (Battisti 1988; Schopf and Suarez 1988, 1990). On the other hand, the amplitudes of model ENSO oscillations can be easily affected by many parameters, e.g., the coupling strength between the ocean and atmosphere. However, the atmospheric spin-up time, a parametrization operating only in the atmosphere and irrelevant to ocean processes, is able to influence the period of coupled oscillations without significantly affecting their amplitudes, although the effects given by the atmospheric spin-up time are more modest compared with the impact given directly from the ocean (i.e., the change of vertical mixing scheme). Using a simple coupled model of Jin (1996), we obtained similar atmospheric time lag effect both numerically and analytically. The analytical derivation is documented in the Appendix of Neelin et al. (1999). The insignificant time lag in the reconstructed wind field given by this parametrization can be lengthened by coupling to significantly change coupled periods. These all suggest that we may need to consider the atmospheric spin-up time quantitatively for ENSO modeling.

3.2.4 Seasonal cycle effect

Figures 10 and 11 represent the same cases as in Figs. 8 and 9, respectively, but with prescribed seasonal cycle. Each NINO3 time series consists of cycles of 2- to 4-year periods, determined by the interval between peaks of two warm phases. To allow the HCM to adjust, the first warm cycle is excluded in examining the coupled ENSO behavior. With the surface-layer parametrization, the ENSO cycles for the case including a no atmospheric spin-up effect (Fig. 10a) tend to lock to a 3-year period. With the atmospheric spin-up time scale of 30 days (Fig. 10b), most cycles have 3-year period, but one has 4-year period. The average period is 3.13 years. With 60-day spin-up time scale (Fig. 10c), the NINO3 series consists of 4-year and 3-year cycles, and an average period of 3.57 years. A NINO3 series with periodic 4-year cycles is obtained with the spin-up time scale of 90 days (Fig. 10d).

Without the surface-layer parametrization, the NINO3 series exhibits a sequence of approximately 2-year and 3-year period events for the case including no atmospheric time scale (Fig. 11a), resulting in a 2.5-year average period. With the spin-up time scale of 30 days (Fig. 11b), the average period is approximately 2.85 years. Many of the cycles have a 3-year period, but occasionally a cycle falls short of three years (indicated by the dot-dashed vertical line), resulting in a warm phase of different seasonal timing and evolution. With the 60-day spin-up time scale (Fig. 11c), ENSO cycles lock to a 3-year period. With the spin-up time of 90 days (Fig. 11d), the average period is 3.25 years. Coupled periods from all experiments discussed above are given in Table 1.

As in cases without the seasonal cycle, the averaged ENSO frequencies tend to increase with spin-up time for both vertical mixing schemes in the presence of the seasonal cycle. In addition, cases with the surface-layer parametrization have longer average periods and larger amplitude than the cases without. Many cases here show frequencies locked to a rational value of the frequency ratio of the ENSO frequency to the annual frequency. For example, the case in Fig. 10c has roughly a 2/7 frequency ratio, and the case in Fig. 11a has a 2/5 frequency ratio.

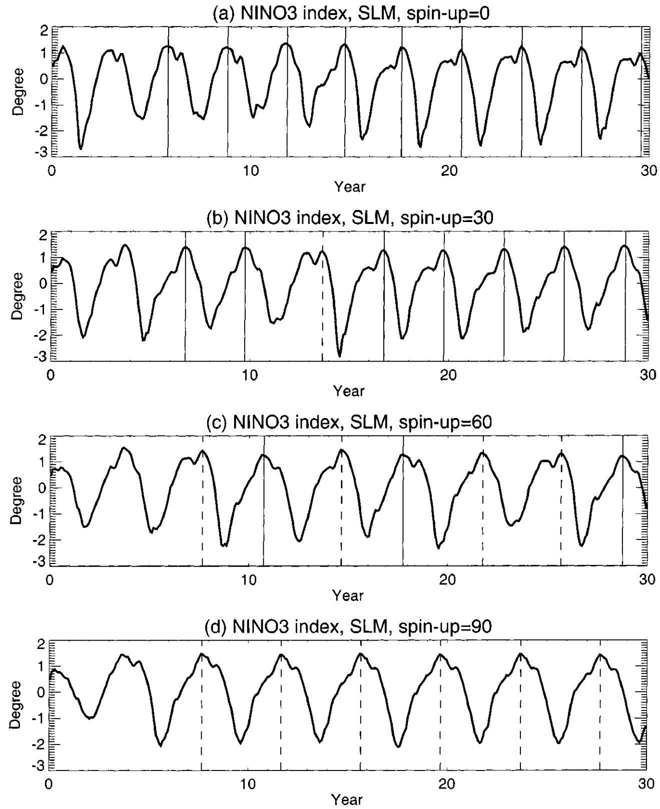

Fig. 10a–d NINO3 indices for SST anomaly, with respect to the mean seasonal cycle, for coupled simulations with the surface-layer parametrization and **a** without the atmospheric spin-up time parametrization, **b** with the atmospheric spin-up time scale of 30 days, **c** with the atmospheric spin-up time of 60 days, and **d** with the atmospheric spin-up time of 90 days. The prescribed seasonal cycle in mean wind fields and heat flux are used in all cases presented here. *Thin solid vertical lines* represent 3-year period cycles, counting from the previous warm peak. The *dashed vertical lines* represent 4-year period cycles

The frequency tends to lock to integer periods that are close to the inherent frequency, as indicated in Bak (1986) and Jin et al. (1994). For example, with the surface-layer parametrization, the inherent period with atmospheric spin-up time of 30 days is 3.35 years, which results in 3-year but sometimes 4-year frequency-locked ENSO cycles when the seasonal cycle is present. With the atmospheric spin-up time of 90 days, the ENSO cycles in the presence of the seasonal cycle show a 4-year period, while the inherent period is 4.05 years. This is also applicable to the cases without the surface-layer parametrization. When the ENSO cycles appear to have 3-year frequency-locking behavior in the presence of the seasonal cycle, the inherent periods can be 2.8 years for the case with the atmospheric spin-up time of 30 days

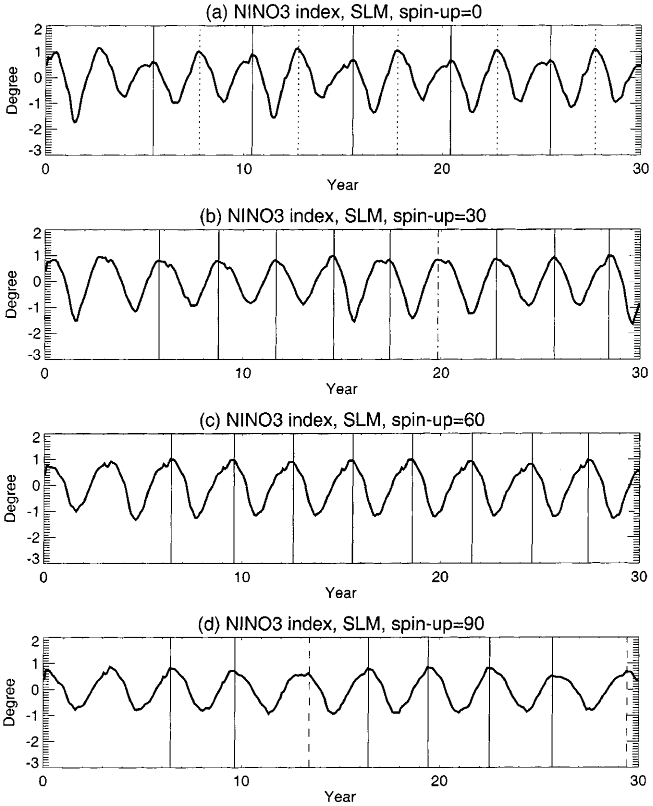

Fig. 11a–d Same as in Fig. 10, except for the case without the surface-layer parametrization. The *dot-dashed vertical line* in **b** represents a 2.5-year period cycle

Table 1 Averaged coupled periods with different atmospheric spin-up time and vertical mixing schemes in 30-year integrations with the seasonal cycle (w/ SC) and without the seasonal cycle (w/o SC)

Spin-up time		Mod-Ri scheme	Mod-Ri + SLM
0 day	w/o SC	2.5	3.0
	w/ SC	2.5	3.0
30 days	w/o SC	2.8	3.35
	w/ SC	2.85	3.13
60 days	w/o SC	3.1	3.71
	w/ SC	3.0	3.57
90 days	w/o SC	3.3	4.05
	w/ SC	3.25	4.0

and also 3.1 years for the case with 60-day spin-up time scale. Nevertheless, although all cases show frequency locking behavior in the presence of the seasonal cycle, most ENSO cycles do not exactly repeat themselves (e.g., Figs. 10a–c and 11b), showing very mild chaotic behavior.

For each vertical mixing scheme, the spatial and temporal features of ENSO oscillation with different atmospheric spin-up times are similar. Therefore, only the detailed spatial and temporal analysis for the case with the surface-layer parametrization and 60-day atmospheric spin-up time scale, defined as the standard version, is given in the next section.

4 The standard version

To define a standard version of the HCM, we need to determine a suitable atmospheric spin-up scale which reflects physical reality and also results in realistic ENSO periods. Since the SVD model is derived from monthly average data, the shortest spin-up time scale that the SVD atmosphere can resolve is 30 days. Over the tropical ocean, moist convective processes are important for atmospheric adjustment and tend to give slow phase speeds. For example, the Madden and Julian oscillation has a time scale of 30–50 days. Thus the atmospheric adjustment over the tropical ocean area appears to have a time scale on the order of 60 days or less. Although 60-days is on the longer side, the HCM results tend to simulate a better ENSO period when a time scale of 60 days is chosen than for a 30-day time scale. A spin-up time scale of 60 days, along with the surface-layer parametrization, is thus selected as the standard model version.

The last 100-year NINO3 time series of a 130-year integration for the case with the standard HCM version is presented in Fig. 12. The time series exhibits a complicated oscillation. During the first 60 years, the ENSO events occur in a sequence of 3-, 4-, 3-, 4-, 4-year cycles, as determined by the interval between the two adjacent warm peaks. In the last 30 years, the ENSO events appear to occur in a sequence of 4- and 3-year cycles. The ENSO cycles seem to frequency lock to different frequency regimes during this 100-year segment.

The spatial structure in SST, heat content and zonal wind stress fields are described by deriving the empirical orthogonal functions (EOFs) from the last 90-year results of the 130-year run. The EOF analysis is done jointly with all three fields while keeping them approximately equal in amplitude by multiplying a weighting value, which is the ratio between the standard deviation of temporally averaged SST anomaly field and that of heat content and zonal wind stress anomaly fields. This weighting effect is then removed from the derived EOF maps in order to recover the relative magnitude of each

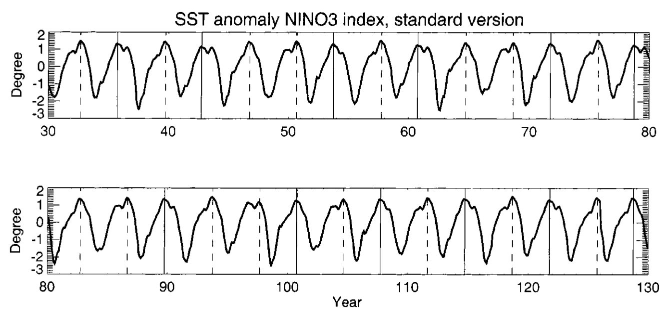

Fig. 12 The last 100-year NINO3 time series of the SST anomalies for a 130-year integration with the standard version of the HCM. *Thin solid vertical lines* represent 3-year period cycles, counted from the previous warm peak. The *dashed vertical lines* represent 4-year period cycles

field. In order to obtain the relative amplitudes between both EOF patterns, we multiply the EOF maps with the standard deviations of the associated principal components. The leading and second EOFs of SST anomalies obtained from the standard version in the presence of the seasonal cycle are shown in Fig. 13a, b. The leading EOF accounts for about 69.7% of the variance and is closely related to the simulated ENSO from the associated time series (time series figures not shown). The second EOF, accounting for 22.3% of the variance,

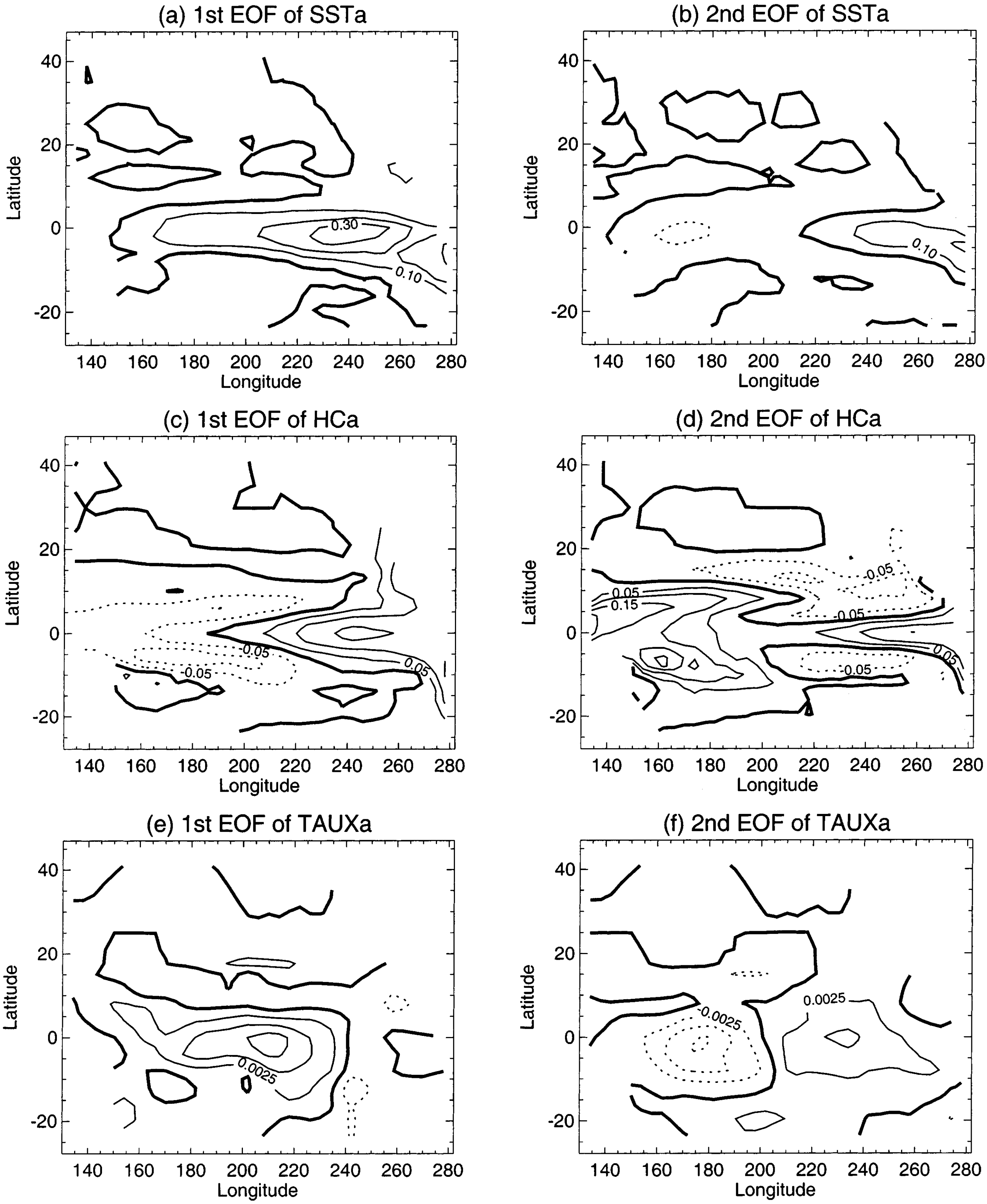

represents the transition phase of ENSO with a quarter-period shift from the leading ENSO phase. Figure 13c, d and e, f are as in Fig. 13a, b, but for heat content and zonal wind stress fields, respectively. An EOF analysis derived separately for each field (figures not shown) is also made for confirmation purposes. The resulting EOF patterns and principal components are similar to those calculated jointly, but with smaller variance percentage, 63.6% for the 1st EOF and 28.3% for the 2nd EOF for both heat content and SST anomaly fields.

During the ENSO phase (1st EOF), a large-scale warming appears centered in the eastern equatorial Pacific. This warming is accompanied by westerly wind anomalies displaced to the west of SST anomalies and centered at the equator approximately 30° east of the dateline. Heat content anomalies are negative in the western Pacific with the strongest signals off the equator and positive at the equator in the central and eastern Pacific, a characteristic asymmetric pattern but with less westward extension. The second EOF of the SST anomaly field shows a westward propagation feature compared to the 1st EOF pattern, and has weaker amplitude. The associated heat content pattern, representing the ocean memory, shows a strong signal propagating into the equatorial wave guide as generated during the preceding cold phase and then reflected at the western boundary, as described in ocean wave dynamics.

5 Conclusions

A hybrid coupled model for the tropical Pacific ocean-atmosphere system is used for ENSO simulations. In this HCM, we use an empirically estimated atmospheric model, which is derived from the first seven coupled modes of a singular value decomposition of the covariance between observed monthly mean surface wind stress and SST fluctuations, containing only interannual variability, coupled to the GFDL modular ocean model (MOM). Two physical parametrizations, neglected in the previous version, are implemented in the HCM: the surface wind mixing and atmospheric time scale.

The parametrization of vertical mixing is crucial in ocean modeling, and here we show that coupled simulations are strongly sensitive to it. Although the ocean boundary layer and interior possess different properties, some models use ocean mixing schemes that parametrize only the ocean interior mixing. In our previous version, we used a modified Richardson-number-dependent (Mod-Ri) vertical mixing scheme for the ocean interior mixing, but did not specifically include the surface wind mixing effect in the ocean boundary layer. In the current HCM, we include a simple parametrization for surface-layer wind mixing, which increases mixing in the surface layer, and tends to deepen it. The inclusion of the surface-layer parametrization results in a longer coupled ENSO period. Without the seasonal cycle, the Mod-Ri scheme with and without the surface-layer parametrization yield an ENSO period of 2.5 years and 2.8 years, respectively. When the seasonal cycle is present, simulated ENSO cycles exhibit frequency locking behavior because of the interaction with the seasonal cycle. With only the Mod-Ri scheme, the ENSO variability locks to a sequence of 2- and 3-year cycles. When the surface-layer parametrization is included, 3-year frequency locking is obtained. The sensitivity of the vertical mixing scheme to ENSO periods is consistent with the result of an intermediate coupled model (Jin and Neelin 1993a, b; Neelin and Jin 1993). Jin et al. (1996) use a parameter that weakens surface-layer currents to lengthen the period of their model ENSO. Here in addition to weaker surface currents, stronger vertical mixing tends to give weaker stratification above the thermocline in the eastern Pacific, which may also contribute to the lengthening of the period.

The other physical parametrization is to include a representation of atmospheric time scale, which represents important processes in the tropical Pacific area but is neglected in the SVD empirical atmospheric model. We represent the atmospheric spin-up time by parametrizing the wind field as coupled to weighted average SST anomalies (with weights exponentially decaying over past time). With a longer atmospheric spin-up time, a longer inherent period is obtained. Examples are given by comparing the coupled results using 30-, 60- and 90-day atmospheric spin-up time scales. Without the seasonal cycle, the inherent ENSO periods are 2.8, 3.1 and 3.35 years without the surface-layer parametrization, and 3.35, 3.71 and 4.05 years with the surface-layer parametrization. With the seasonal cycle, the simulated ENSO oscillation tends to frequency lock to those integer-year frequencies which are closest to their inherent periods. For example, with the Mod-Ri mixing scheme, most ENSO frequencies lock to 2 and 3 years, and with the surface-layer parametrization, 3- and 4-year frequency locking behaviors are found. Longer average ENSO periods are obtained with the longer atmospheric spin-up time scales for both mixing schemes. These results show that a small spin-up time in the wind field (e.g., 30 days) can be lengthened by coupling to have more significant impact on ENSO period (3–4 months). A potential importance of atmospheric time scale in ENSO modeling is indicated, especially for simple atmospheric models.

Atmospheric time scales are much shorter than those of the ocean. The longest time scale known in tropical atmosphere is the Madden and Julian Oscillation with a period of 30 to 50 days. On the other hand, our SVD model, using monthly mean data, can only resolve time

Fig. 13a–f The joint EOF patterns of SST, heat content and zonal wind stress anomalies for the standard case. **a** The first and **b** second EOFs for SST anomalies; **c** the first and **d** second EOFs for heat content anomalies; **e** the first and **f** second EOFs for zonal wind stress anomalies. *Solid lines* represent positive values and *dashed lines* represent negative values scales longer than 30 days. We typically consider values of the atmospheric spin-up time in the range of 30–60 days. This also provides a convenient parameter for sensitivity testing that does not affect ocean climatology. It happens that a value of 60-days gives the most realistic coupled periods. We thus define the "standard" version of the HCM as one which includes the surface-layer parametrization in addition to the Mod-Ri vertical mixing scheme, and with the atmospheric spin-up time scale of 60 days. The standard version of the coupled model exhibits complicated oscillation behavior. For example, the NINO3 time series for the last 100 years of a 130-year integration exhibits two stages of oscillation. The first stage lasts for 60 years and contains 3 repeated sequences. Each of the 18-year sequences in turn contains 5 ENSO cycles. These 5 ENSO cycles are arranged as 3-year, 4-year, 3-year, and two 4-year events. In the second stage, the model exhibits a pattern of 4-year and 3-year ENSO cycles.

The structure of the ENSO oscillations with the standard version is described by the first 2 EOF patterns from the last 90-year simulated data of the 130-year run. The first EOF pattern, the mature phase ENSO mode, accounts for 69.7% of the total variance. With the maxima in the eastern Pacific, SST anomalies develop in phase with the deepened thermocline in the east and shallow thermocline in the west. Maximum westerly anomalies are located in the central Pacific, slightly west of the maximum SST anomaly. The second EOF pattern, accounting for 22.2% of the total variance, shows the transition mode and leads the mature phase by approximately one quarter of the period. The SST anomaly pattern in the transition phase is relatively weak, with an initial warming signal appearing in the southeastern Pacific. The heat content anomaly field shows a structure typical of ocean memory as a result of wave dynamics. The overall features shown by the standard HCM are consistent with the mixed-SST/ocean-dynamics mode behavior.

Overall, the spatial form and evolution of the anomalies from phase to phase of the oscillation are robust as the physical parametrizations are changed. This indicates that the basic physical mechanism is essentially the same as parameters are varied in this realistic range. The main change is the increase or decrease of period which occurs by slight modifications of processes within the same behavior regime. The changes in the inherent ENSO period do produce changes in frequency locking behavior. For the physical parametrizations considered here, the sensitivities may thus be ranked as follows: (1) detailed aspects of the time evolution such as frequency and phase-locking are most sensitive; (2) the period can be affected considerably; (3) but the underlying oscillation mechanism is basically unchanged.

Acknowledgements This work was supported in part by National Oceanography and Atmosphere Administration (NOAA) grant NA56GP0451 and NA86GP0314, and National Science Foundation grant ATM-9521389. Computations were carried out at the National Center for Atmospheric Research, which is sponsored by NSF, and at the Florida State University Computer Center, sponsored by the NOAA climate and global change program. We thank D. Gutzler for providing the SVD code, B. Blanke for providing the modified mixing and solar penetration schemes, and C. Perigaud for discussions. We also thank Dr. Lee-Lueng Fu at the Jet Propulsion Laboratory/California Institute of Technology for supporting HHS in finishing this paper at JPL.

Appendix A

Modified Richardson-number-dependent vertical mixing scheme and solar penetration scheme

The Pacanowski and Philander (1981, PP) Richardson-number dependent vertical mixing scheme is tuned to reproduce the main characteristics of an equatorial basin, such as the mixed layer depth, the zonal slope of the thermocline and the structure of the equatorial undercurrent, but is known to generate insufficient vertical mixing in the mixed layer and thus leads to some deficiencies in both coupled and uncoupled seasonal cycle in the HCM. A new formulation for both vertical eddy viscosity coefficient (K_m) and vertical eddy diffusivity coefficient (K_ρ), with still a dependence on the local Richardson number is derived by B. Blanke (1993, personal communication).

$$\begin{aligned} &\text{if} \quad \mathrm{Ri} \le 0.2, \quad K_m = K_\rho = 10^{-1}\ \mathrm{m^2\,s^{-1}} \\ &\text{if} \quad \mathrm{Ri} > 0.2, \quad K_m = 5.12 \times 10^{-8}\ \mathrm{Ri}^{-9} + 10^{-6}\ \mathrm{m^2\ s^{-1}} \\ &\qquad\qquad\qquad\quad\ K_\rho = 1.02 \times 10^{-8}\ \mathrm{Ri}^{10} + 10^{-7}\ \mathrm{m^2\ s^{-1}} \end{aligned}$$

These new relationships attempt to mimic the results obtained by Peters et al. (1988) in their direct measurements of equatorial oceanic turbulence and the results obtained by Blanke and Delecluse (1993) with a more sophisticated turbulence closure scheme. In principal, the new formulation allows larger mixing in high turbulent regions (small Ri) and smaller mixing in low turbulent regions (large Ri) than the PP scheme. The observed relationship that there is a sharp increase of turbulence when the Richardson number is lower than a critical value (close to 0.23) is coarsely included in the new formulation. The molecular thresholds obtained for large values of Ri are the same as before. Since this scheme is still Richardson-number dependent, we refer to it as the Modified Richardson-number-dependent scheme (Mod-Ri).

The eddy viscosity and diffusivity for the PP and the Mod-Ri schemes are shown in Fig. A1.

The modification of the analytical relations for K_m and K_ρ has been associated with the implementation of an algorithm to account for the penetration of solar radiation in the ocean. Paulson and Simpson's (1977) parametrization for vertical irradiance is used in the ocean for this purpose. For most general studies of the oceanic circulation and variability, the parameters corresponding to a seawater of type I ($R = 0.58$,

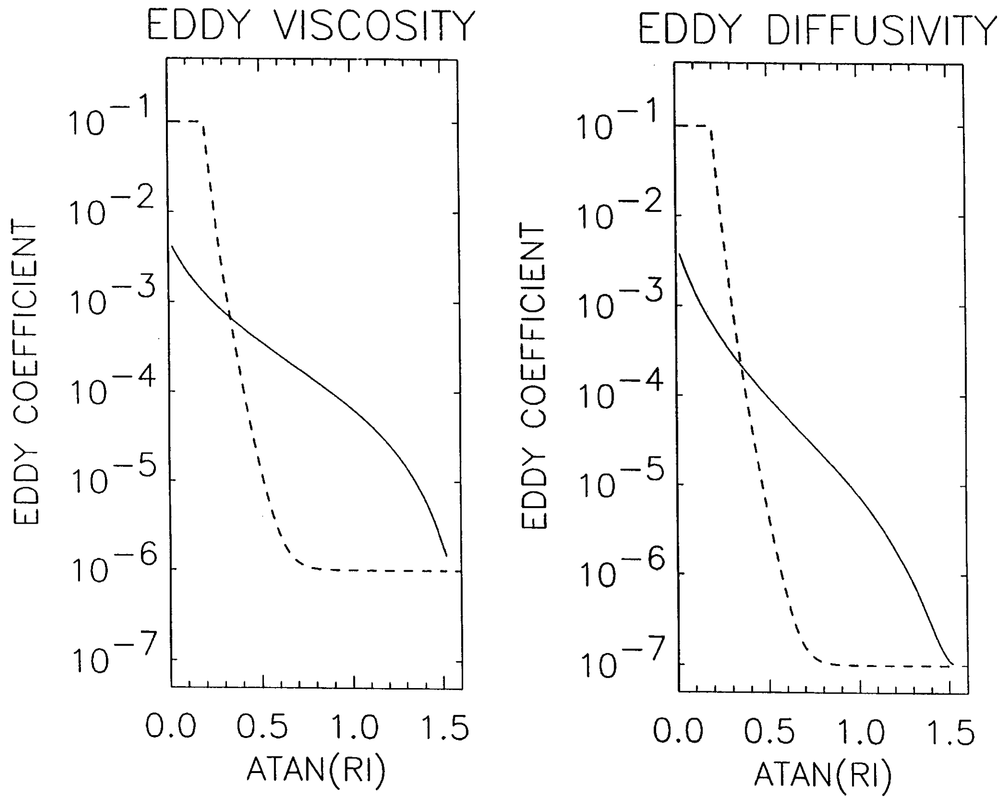

Fig. A1 Eddy viscosity and diffusivity coefficients for the PP scheme (*solid line*) and the Mod-Ri scheme (*dashed line*). Units $m^2\ s^{-1}$

$\xi_1 = 0.35$ m, $\xi_2 = 23$ m) are usually chosen, as in Rosati and Miyakoda (1988). We also follow this choice.

These two modifications in the mixed layer physics have been tested in various simulations of the tropical Pacific Ocean. The impact is found to be in agreement with other sensitivity experiments (e.g., Blanke and Delecluse 1993).

References

Anderson DLT, McCreary JP (1985) Slowly propagating disturbances in a coupled ocean-atmosphere model. J Atmos Sci 42:615–629

Bak P (1986) The Devil's staircase. Physics Today Dec. 1986: 38–45

Balmaseda MA, Anderson DLT, Davey MK (1994) ENSO prediction using a dynamical ocean model coupled to statistical atmospheres. Tellus 46A:497–511

Barnett TP, Latif M, Graham N, Flügel M, Pazan S, White W (1993) ENSO and ENSO-related predictability. Part I: prediction of equatorial Pacific sea surface temperature with a hybrid coupled ocean-atmosphere model. J Clim 6:1545–1566

Battisti DS (1988) The dynamics and thermodynamics of a warming event in a coupled atmosphere-ocean model. J Atmos Sci 45:2889–2919

Battisti DS, Hirst AC (1989) Interannual variability in the tropical atmosphere/ocean system: influence of the basic state, ocean geometry and nonlinearity. J Atmos Sci 46:1687–1712

Blanke B, Delecluse P (1993) Variability of the tropical Atlantic ocean simulated by a general circulation model with two different mixed layer physics. J Phys Oceanogr 23:1363–1388

Blanke B, Neelin JD, Gutzler D (1997) Estimating the effect of stochastic wind stress forcing on ENSO irregularity. J Clim 10: 1473–1485

Cane MA, Münnich M, Zebiak SE (1990) A study of self-excited oscillations of the tropical ocean-atmosphere system. Part I: linear analysis. J Atmos Sci 47:1562–1577

Cane MA, Zebiak SE (1985) A theory for El Niño and the Southern Oscillation. Science 228:1084–1087

Chang P, Ji L, Wang B, Li T (1995) Interactions between the seasonal cycle and El Niño-Southern Oscillation in an intermediate coupled ocean-atmosphere model. J Atmos Sci 52: 2353–2372

Chang P, Wang B, Li T, Ji L (1994) Interactions between the seasonal cycle and the Southern Oscillation – frequency entrainment and chaos in an intermediate coupled ocean-atmosphere model. Geophys Res Lett 21:2817–2820

Cox MD (1984) A primitive equation, 3-dimensional model of the ocean. GFDL Ocean Group Technical Rep 1, GFDL/NOAA, Princeton, New Jersey, USA

Deser C, Wallace JM (1990) Large-scale atmospheric circulation features of warm and cold episodes in the tropical Pacific. J Clim 3:1254–1281

Eckert C, Latif M (1997) Predictability of a stochastically forced hybrid coupled model of the tropical Pacific ocean-atmosphere system. J Clim 10:1488–1504

Hao Z, Neelin JD, Jin F-F (1993) Nonlinear tropical air-sea interaction in the fast-wave limit. J Clim 6:1523–1544

Iooss G, Joseph DD (1990) Elementary stability and bifurcation theory. Springer, New york, Berlin Heidelberg, pp 324

Jensen MH, Bak P, Bohr T (1984) Transition to chaos by interaction of resonances in dissipative systems. Part I. Circle maps. Physical Rev A 30:1960–1969

Jin F-F (1996) An equatorial recharge paradigm for ENSO. Part I: conceptual model. J Atmos Sci 54:811–829

Jin F-F, Neelin JD (1993a) Modes of interannual tropical ocean-atmosphere interaction – a unified view. Part I: numerical results. J Atmos Sci 50:3477–3503

Jin F-F, Neelin JD (1993b) Modes of interannual tropical ocean-atmosphere interaction – a unified view. Part III: analytical results in fully-coupled cases. J Atmos Sci 50: 3523–3540

Jin F-F, Neelin JD, Ghil M (1994) El Niño on the "Devil's Staircase": annual subharmonic frequency locking and ENSO aperiodicity. Science 264: 70–72

Jin F-F, Neelin JD, Ghil M (1996) El Niño/Southern Oscillation and the annual cycle: subharmonic frequency locking and aperiodicity. Physica D 98: 442–465

Large WG, McWilliams JC, Doney SC (1994) Oceanic vertical mixing: a review and a model with a non-local K-profile boundary layer parametrization. Rev Geophys 32: 363–403

Latif M, Flügel M (1991) An investigation of short-range climate predictability in the tropical Pacific. J Geophys Res 96: 2661–2673

Latif M, Villwock A (1990) Interannual variability as simulated in coupled ocean-atmosphere models. J Mar Syst 1: 51–60

Latif M, Stockdale T, Wolff J, Burgers G, Maier-Reimer E, Junge MM, Arpe K, Bengtsson L (1994) Climatology and variability in the ECHO coupled GCM. Tellus 46A: 351–366

Legler DM, O'Brien JJ (1984) Atlas of tropical Pacific wind stress climatology 1971–1980. Department of Meteorology, Florida State University, Tallahassee, Florida, pp 182

Levitus S (1982) Climatological atlas of the world ocean. NOAA Prof Pap 13, 173 pp, 17 microfiche, US Government Printing Office, Washington, D.C., USA

Neelin JD (1991) The slow sea surface temperature mode and the fast-wave limit: analytic theory for tropical interannual oscillations and experiments in a hybrid coupled model. J Atmos Sci 48: 584–606

Neelin JD, Jin F-F (1993) Modes of interannual tropical ocean-atmosphere interaction – a unified view. Part II: analytical results in the weak-coupling limit. J Atmos Sci 50: 3504–3522

Neelin JD, Jin F-F, Syu H-H (1999) Variations in ENSO phase-locking. J Climate, in press.

Oberhuber JM (1988) An atlas based on the COADS data set: the budgets of heat buoyancy and turbulent kinetic energy at the surface of the global ocean. Max-Planck-Institut für Meteorologie Rep 15, Hamburg, Germany

Pacanowski RC, Philander SGH (1981) parametrization of vertical mixing in numerical models of the tropical oceans. J Phys Oceanogr 11: 1443–1451

Paulson CA, Simpson JJ (1977) Irradiance measurements in the upper ocean. J Phys Oceanogr 7: 952–956

Peters H, Gregg MC, Toole JM (1988) On the parametrization of the equatorial turbulence. J Geophys Res 93: 1199–1218

Rasmusson EM, Carpenter TH (1982) Variations in tropical sea surface temperature and surface wind fields associated with the Southern Oscillation/ El Niño. Mon Weather Rev 110: 354–384

Reynolds RW (1988) A real-time global sea surface temperature analysis. J Clim 1: 75–86

Rosati A, Miyakoda K (1988) A general circulation model for the upper ocean simulation. J Phys Oceanogr 18: 1601–1626

Schopf PS, Suarez MJ (1988) Vacillations in a coupled ocean-atmosphere model. J Atmos Sci 45: 549–566

Schopf PS, Suarez MJ (1990) Ocean wave dynamics and the time scale of ENSO. J Phys Oceanogr 20: 629–645

Seager R, Zebiak SE, Cane MA (1988) A model of the tropical Pacific sea surface temperature climatology. J Geophys Res 93: 1265–1280

Suarez MJ, Schopf PS (1988) A delayed action oscillator for ENSO. J Atmos Sci 45: 3283–3287

Syu H-H, Neelin JD, Gutzler D (1995) Seasonal and interannual variability in a hybrid coupled GCM. J Clim 8: 2121–2143

Tziperman E, Cane MA, Zebiak S (1995) Irregularity and locking to the seasonal cycle in an ENSO prediction model as explained by the quasi-periodicity route to chaos. J Atmos Sci 52: 293–306

Tziperman E, Stone L, Cane MA, Jarosh H (1994) El Niño chaos: overlapping of resonances between the seasonal cycle and the Pacific ocean-atmosphere oscillator. Science 246: 72–74

Waliser DE, Blanke B, Neelin JD, Gautier C (1994) Shortwave feedbacks and El Niño-Southern Oscillation: forced ocean and coupled ocean-atmosphere experiments. J Geophys Res 99: 25109–25125

Zebiak SE, Cane MA (1987) A model EI Nino Southern Oscillation. Mon Wea Rev, 115: 2262–2278